Characterisation of the Mechanical and Oxygen Barrier Properties of Microfibril Reinforced Composites

by

Ryan John Shields

A thesis submitted in partial fulfilment of the requirements for the degree of Doctor of Philosophy in Engineering

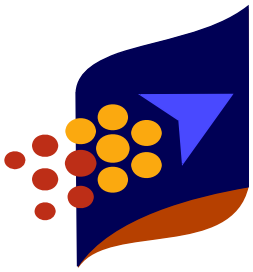

Centre for Advanced Composite Materials

THE UNIVERSITY OF AUCKLAND

November 2008

Abstract

A relatively new type of reinforced composite material, derived from immiscible blends of thermoplastic homopolymers, is characterised in this doctoral research. Microfibril Reinforced Composites (MFCs) utilise common engineering and commodity polymers to create high strength and stiffness microfibrils dispersed in an isotropic matrix. Unlike traditional polymer composites, MFCs use the dispersed component of a blend to create an even distribution of *in situ* reinforcing microfibrils via a simple extrusion, drawing and processing technique.

This research quantifies the mechanical and oxygen gas barrier properties of polyolefin-based MFCs containing polyethylene terephthalate (PET) microfibrils. It is concerned not only with identifying MFCs with the best properties, but also with how manufacturing parameters influence those properties.

Characterisation is split into several parts. Initial investigations into blend development during extrusion and drawing were conducted. The main purpose of this was to gain a

better understanding of the factors influencing the morphological changes that occur during production. Blend viscosity ratio and capillary number were identified as key factors in determining the onset of coalescence, deformation and break up of the dispersed polymer. The effects on microfibril formation of several important manufacturing parameters were highlighted, with die diameter and extrusion speed the most influential of these. A significant skin-core microstructure was observed. Formation of elongated microfibres (with negligible molecular chain alignment) was shown to occur during extrusion, which was subsequently justified via modelling of the shear stress flow fields in the die.

Drawn blends gave very high tensile strengths and stiffnesses due to highly oriented molecular chains. A threshold draw ratio of 3.5, at which properties change considerably, was identified. Mechanical properties of injection moulded MFCs from polypropylene were not considerably better than the neat matrix polymer. However, those from polyethylene (PE) showed significant improvement via injection moulding and directional compression moulding. MFCs with just 30% microfibril content displayed tensile properties up to six times greater than neat PE.

Measurements of oxygen gas permeability highlighted improvements of up to 65%. Processing and cooling conditions were shown to significantly influence permeability via a Taguchi experimental design analysis. MFC storage containers from PE/PET were injection moulded as proof-of-concept on completion of the research.

Acknowledgements

First and foremost, I would like to thank my wonderful girlfriend Nicola for all her love and support throughout my studies. Your words of encouragement and advice have done much to lighten the load over these last few years. Thank you for having the patience and commitment to delay your travels for me. Your new found appreciation for plastics and plastic composites also gives me great pride.

To Mum, Dad, Kirstin and Caroline. Thank you for your encouragement and support, and for being there whenever I needed you.

Prof. Debes Bhattacharyya, your dedication, guidance and feedback, not to mention your extensive manufacturing and composites knowledge, have been invaluable in assisting me throughout my years under your supervision.

Many thanks are also extended to Prof. Stoyko Fakirov. Your patience whilst I learnt the fundamentals of polymer chemistry and processing, as well as your willingness and proficiency at explaining both the fundamentals and intricacies of MFCs is greatly appreciated. I would also like to thank Assoc. Prof. Allan Easteal for his guidance on several chemistry related issues.

A very big thanks to the technicians who assisted me during my work – Rex, Jos, Callum, Steve, Shane and Catherine. Especially to Rex, whose knowledge of polymers and vast expertise in their processing was invaluable to me.

I would also like to acknowledge support of this research by the Foundation for Research, Science and Technology New Zealand through funding Grant #UOAX0406.

Cheers to Scott for his careful proofreading of my manuscript.

Finally, a huge thank you to my friends and colleagues at CACM (both past and present), especially Anu, Sandra, Lynley, Peter, Jim, Quentin, Rehan and Sanjeev. Whether it was small scale fibreboard explosions, lost fluoropolymers, online comic strips or all manner of lunchtime conversation topics, you all helped to make my stay at CACM thoroughly memorable and enjoyable.

TABLE OF CONTENTS

Abstract ii

Acknowledgements iv

List of Tables xi

List of Figures xiii

Nomenclature xviii

Glossary of Terms & Abbreviations xxi

1 Introduction **1**

2 Literature Review **6**

2.1 Polymer Blending and Composites 7

2.1.1 A brief history of blending 7

2.1.2 Reasons for blending 9

2.1.3 Miscibility and compatibility 11

2.1.4 The importance of blending 13

2.1.5 Types of mixing 15

2.1.6 Polymer composites 16

2.2 What are Microfibril Reinforced Composites? 18

2.2.1 Background 18

2.2.2 Manufacturing methodology 21

2.2.3 Mechanical properties 24

2.2.4 Factors that influence MFC properties 30

2.2.4.1 Reinforcing content 31

2.2.4.2 Drawing 32

2.2.4.3 Molecular orientation 34

2.2.4.4 Fibril size and shape 35

2.2.4.5 Interfacial adhesion 36

2.2.4.6 Moulding techniques 37

2.2.5 Common characterisation methods 38

2.2.6 Application of property prediction methods to MFCs 39
2.2.7 Transcrystallisation 41
2.2.8 Compatibilisation 43
2.2.8.1 Addition of a synthesised copolymer 43
2.2.8.2 Self-compatibilisation 45
2.3 Analysis of the MFC Manufacturing Process 47
2.3.1 Processing techniques 47
2.3.2 Types of flow 49
2.3.3 Forces in the melt 49
2.3.4 Characteristic blend parameters 50
2.3.5 Droplet formation and coalescence 52
2.3.6 Stability and break-up mechanisms 56
2.3.7 Morphology development 58
2.3.8 Drawing 60
2.4 Barrier Properties of Polymer Blends and Composites 62
2.4.1 Background 62
2.4.2 Theory 63
2.4.3 Methods of barrier enhancement 65

3 Manufacturing, Testing & Analysis Techniques 66

3.1 Background 66
3.2 Manufacturing Setup 69
3.2.1 Materials 69
3.2.2 Mixing and extrusion 70
3.2.3 Drawing 72
3.2.4 Processing 74
3.2.4.1 Compression moulding 75
3.2.4.2 Injection moulding 78
3.3 Mechanical Testing Setup 80
3.3.1 Filaments 81
3.3.2 Moulded specimens 82
3.3.3 Films 83
3.4 Oxygen Permeability Testing Setup 84
3.5 Analysis Techniques 89
3.5.1 Scanning Electron Microscopy 89
3.5.1.1 Particle measurement and analysis 90
3.5.2 Energy Dispersive X-ray Spectroscopy 90

3.5.3 Differential Scanning Calorimetry 92
3.5.4 Rheometer 93
3.5.5 Shrinkage measurement 94
3.6 Experimental Design using the Taguchi Method 95
3.7 Concluding Remarks 98

4 Blend Development 99

4.1 Analysis of Polymers 100
4.1.1 Glass transition and melting temperatures 100
4.1.2 Thermodynamic immiscibility 101
4.1.3 Viscosity 102
4.1.4 Viscosity ratio 102
4.2 Microfibres or Microfibrils? 104
4.3 Observation of Microfibre Formation during Extrusion 107
4.4 Effect of Extrusion Speed on Microfibre Formation 109
4.5 Influence of Die Diameter and L/D Ratio on Particle Dimensions 113
4.6 Die Swell and the Effect of Extrusion and Drawing on Microfibril Dimensions and Blend Tensile Strength 117
4.7 Tensile Properties and the Effect of Drawing Temperature 123
4.8 Modelling the Flow Through a Conical Extrusion Die 127
4.8.1 Introduction 127
4.8.2 Calculation of the spherical velocity field model 129
4.8.3 Calculation of the triangular velocity field model 131
4.8.4 Extension to a spherical shear stress model 136
4.8.5 How do these models apply to MFC development? 139
4.9 Concluding Remarks 140

5 Mechanical Characterisation 142

5.1 Properties of PE/PET Blends 143
5.1.1 Manufacturing parameters 143
5.1.2 Results and discussion 144
5.2 Properties of Injection Moulded PP/PET 146
5.2.1 Manufacturing parameters 146
5.2.2 Results and discussion 152
5.2.3 Composite morphology from SEM 156

5.2.4 Taguchi analysis 158
5.2.4.1 Factor effects and Q-Q plots 159
5.2.4.2 Analysis of Variance (ANOVA) 166
5.2.4.3 What does Taguchi analysis tell us about these MFCs? 168
5.2.5 Compatibilisation 168
5.3 Properties of Compression Moulded PE/PET 171
5.3.1 Alteration of the composite reinforcing fraction 171
5.3.2 Effect of microfibril orientation 173
5.4 Concluding Remarks 177

6 Oxygen Barrier Properties 180

6.1 Permeability Calculations 180
6.2 Preliminary Permeation Experiments 184
6.2.1 Effect of PET content 184
6.2.2 Effect of draw ratio 186
6.3 Composite Film Permeability Investigation 188
6.3.1 Manufacturing parameters 188
6.3.2 Results and discussion 190
6.3.3 Taguchi analysis - permeability 194
6.3.3.1 Factor effects 194
6.3.3.2 Analysis of Variance (ANOVA) 196
6.3.4 Film morphology 196
6.3.5 Mechanical Properties of Films 199
6.3.6 Taguchi analysis - mechanical 200
6.3.6.1 Factor effects 200
6.3.6.2 Analysis of Variance (ANOVA) 203
6.4 How Crystallinity Affects Permeability 205
6.5 The Role of Ageing 208
6.6 MFC Permeability Modelling 211
6.7 Concluding Remarks 217

7 MFC Applications 220

7.1 Prototype MFC Containers 220
7.1.1 Designing the mould set 221
7.1.2 Container production 223
7.1.3 Results 224

7.1.3.1 Oxygen permeability 224
7.1.3.2 Monitoring the pH of milk stored in MFC containers 226
7.2 In What Other Applications could the MFC Concept be Applied? 228
7.2.1 Recycling of blended plastic waste streams 228
7.2.2 Nanofibrillar structures and tissue scaffolding 229
7.2.3 Electroconductive materials 230

8 Conclusions 231

8.1 Conclusions 231
8.2 Achievements & Recommendations for Future Work 234
8.2.1 List of Publications 234
8.2.2 Recommendations for Future Work 235

9 References 237

Appendix A – Flow Modelling Matlab Code A1
Appendix B – Extruder Input Power Calculations B1
Appendix C – Supplementary Taguchi Data C1
Appendix D – Taguchi Analysis of Variance D1

List of Tables

Table 2-1: Mechanical properties, preparation and testing details of MFCs – as reported in reviewed literature 25
Table 2-2: Oxygen permeability of assorted polymers [94] 63
Table 3-1: Temperature profiles used during extrusion 71
Table 3-2: MFC film pressing parameters 77
Table 3-3: Permeability test parameters 88
Table 4-1: Glass transition T_g and melting temperatures T_m of neat materials, blend filaments and MFCs as revealed by DSC thermal analysis 100
Table 4-2: Manufacturing parameters 107
Table 4-3: Manufacturing parameters 109
Table 4-4: Screw speed and resulting core/skin microfibre diameters 110
Table 4-5: Manufacturing conditions 113
Table 4-6: Diameters of microfibres/particles observed in the core/skin of extruded PE/PET filaments for a range of different sized dies 114
Table 4-7: Manufacturing parameters 117
Table 4-8: Diameters and reduction ratios of drawn filaments of PE/PET=70/30 119
Table 4-9: Manufacturing parameters 123
Table 4-10: Measured and theoretical values of thermal expansion (contraction) during cooling 124
Table 4-11: Critical values of extrusion shear stress above which PET microfibres are expected to remain stable 138
Table 5-1: Manufacturing parameters 143
Table 5-2: Factors and levels used for PP/PET experimental design 147
Table 5-3: Parameter combinations for PP/PET experimental design trials 147
Table 5-4: Summary of manufacturing Taguchi analysis of variance results 167
Table 5-5: Manufacturing parameters 169
Table 5-6: Manufacturing parameters 171
Table 5-7: Manufacturing parameters 173
Table 6-1: Verification that permeability is independent of film thickness for MFCs within the test range 182
Table 6-2: Manufacturing parameters 184
Table 6-3: Manufacturing parameters 186

Table 6-4: Experimental design factors and their respective levels 188
Table 6-5: Parameter combinations for PE/PET oxygen permeability trials 189
Table 6-6: Oxygen Gas Transmission Rate (O_2GTR) for films from PE/PET=70/30 191
Table 6-7: Oxygen Permeance ($P'O_2$) for films from PE/PET=70/30 191
Table 6-8: Oxygen Permeability Coefficient (PO_2) for films from PE/PET=70/30 192
Table 6-9: Details for films from PE/PET=70/30 192
Table 6-10: Summary of Taguchi analysis of variance results for oxygen permeability 196
Table 6-11: Summary of Taguchi analysis of variance results for film tensile properties 203
Table 6-12: Enthalpy of fusion and corresponding crystallinity for the PE in various films 206
Table 6-13: Permeability reductions for neat PE and composite films after aging for ~12000 hours 209
Table 7-1: Manufacturing parameters 223

List of Figures

Figure 2-1: Principal aims of polymer blending in recent decades, adapted from [10]. 8
Figure 2-2: World market share of major polymer resins (1995-2000). Commodity resins (blue shades) account for 79% of all plastics. Compiled from [10]. 9
Figure 2-3: Different reinforcements have different effects on material properties: (i) drops can improve impact resistance; (ii) sheets can enhance barrier properties; (iii) fibres can increase tensile strength; (iv) co-continuous phases can improve electrical conductivity. 15
Figure 2-4: Types of mixing of immiscible polymer blends [17]. 16
Figure 2-5: Typical structure of an MFC: (i) composite fracture surface after compression moulding [37]; (ii) reinforcing fibrils after extraction of the matrix polymer [38]. 18
Figure 2-6: Timeline of the development of MFCs. Compiled from [39-43]. 19
Figure 2-7: Potential advantages of using MFCs instead of more traditional polymer composites. 20
Figure 2-8: Flow diagram of the MFC production process. 22
Figure 2-9: Effect of draw ratio on diameter of PP/PET=85/15 wt.% filament (top) and resulting PET fibril diameter (below) [49]. 32
Figure 2-10: Schematic illustrating the changes occurring in the molecular orientation of an MFC and its components during production. 35
Figure 2-11: Cross-section of PP/PET=80/20 blend filament after extrusion. PET fibres are visible in the skin region (left) and PET spheres are visible in the core region (right) [60]. 36
Figure 2-12: TEM micrograph showing transcrystalline layer in ultra-thin section of injection moulded LDPE/PET=50/50 (wt.%) MFC. The white region near the PET surface is a result of the material preparation procedure [67]. 42
Figure 2-13: Effect of compatibiliser on reinforcing fibril formation. 45
Figure 2-14: Transreactions and additional condensation reactions occur during self-compatibilisation of condensation polymers [15]. 46
Figure 2-15: Polymers and their composites are processed using a variety of techniques. MFCs utilise extrusion as well as injection moulding (left) or compression moulding (right) [74]. 47
Figure 2-16: Relationship between droplet behaviour and κ/κ_{cr} 52
Figure 2-17: Coalescence (or break-up) occurring during extrusion. The boxes indicate well aligned PET particles and the arrows point towards complete microfibres. It is common to have both in the one extrudate. 54
Figure 2-18: Coalescence of the dispersed phase can form either (i) strings or (ii) larger drops 54
Figure 2-19: Steps of string formation [23] 55

Figure 2-20: Optical micrographs of a PA6 fibre breaking up inside a PS matrix at 230°C. Initial fibre diameter was 46 microns [83]. 57
Figure 2-21: Relationship between extension and applied force during drawing of a blend filament. 61
Figure 2-22: Molecular alignment via drawing is proven by WAXS imaging [38]. 61
Figure 3-1: Manufacturing an MFC is a three stage process including melt-blending with extrusion, drawing and processing. 67
Figure 3-2: Molecular structures of polymers used. 70
Figure 3-3: PET (left) and PP (right). 70
Figure 3-4: Manufacturing setup. 71
Figure 3-5: A single screw extruder was used (left) to compound and extrude the blends and a heating tunnel with eight pairs of IR lamps was used for drawing (right). 72
Figure 3-6: Extruded filament is collected on spools (left) and then drawn (right). The arrow indicates the point of necking from undrawn diameter (D_u) to drawn diameter (D_d). 74
Figure 3-7: Compression moulded dog-bones were produced using a four part brass mould consisting of two male punches, a female base and a spacer plate. 75
Figure 3-8: MFC sheets were made via compression moulding of continuous filament at 180°C. Tensile specimens were machined from these sheets for properties testing. 76
Figure 3-9: For pressing into films, MFC sheets were cut into segments (left). A template (centre) was used to create the correct film profile (right). 77
Figure 3-10: PE/PET blend pellets ready for injection moulding into MFCs. 79
Figure 3-11: Instron universal testing machine 5567 performing a filament tensile test (left). On the right is an Instron 1185 containing a fractured dog-bone specimen and mechanical extensometer. 80
Figure 3-12: Grips used in Instron for testing filament strength (left) and stiffness (right). 81
Figure 3-13: Three point bend test configuration (left); Charpy impact testing machine (right). 83
Figure 3-14: Permeability testing apparatus. The film is placed between the upper and lower chambers. A sensor monitors the level of oxygen in the measuring chamber. 84
Figure 3-15: Schematic diagram of permeability testing setup. 85
Figure 3-16: Plot showing the level of oxygen in the test cell before and during permeability testing. Gas transmission rate is calculated from the gradient of the steadystate portion of graph ($\Delta y/\Delta t$). 87
Figure 3-17: Example of an SEM panorama used during analysis. 90
Figure 3-18: Location of EDS sites used to identify the fibril/matrix polymers. 91
Figure 3-19: EDS scans of the areas marked in Figure 3-18. The matrix scan (left) shows negligible oxygen, indicating PE. The reinforcing fibrils (right) show oxygen, confirming they are PET. 91
Figure 4-1: DSC scans showing heat capacities of filaments and films of PE/PET as well as thermal properties of the neat materials. 101
Figure 4-2: Changes in viscosity with increasing shear rates for the main polymers used during this research. Tests were at 220°C and 260°C (where possible). 102
Figure 4-3: Viscosity ratio of PET/PP and PET/PE blends with increasing shear rate. 103
Figure 4-4: PET microfibres (left) display good wetting and distribution and can be of similar diameters to drawn microfibrils (right). This can make it difficult to distinguish between the two. 104

Figure 4-5: Blend morphologies immediately after extrusion for four different polymer blends, showing the potential for both drops and microfibres to form under different processing conditions. 106
Figure 4-6: Specimen locations for fibre formation experiment. 107
Figure 4-7: In a blend of PE/PET the dispersed PET particles that exist in the barrel (A) and the die (B) are shaped by the shearing forces of the convergent flow as they transit the die exit (C), transforming into uniformly distributed PET microfibres (D). 108
Figure 4-8: PE throughput for various extruder screw speeds. 110
Figure 4-9: Average fibre diameters in filament core (left) and skin (right) after extrusion at various throughputs. 111
Figure 4-10: Differences in morphology as seen under SEM during examination of the core (left) and skin (right) of a PE/PET blend. Extrusion was at 4.97 g/min. 111
Figure 4-11: Cross-section of a die showing diameter *d* and land length *l*. 113
Figure 4-12: Plots of the average microfibre/particle diameter distributions for PE/PET filaments. 115
Figure 4-13: After extrudate solidification, die swell as a function of increasing die diameter for PE blends containing 30% PET appears to follow the relationship $B = d^{-1/2}$ 119
Figure 4-14: Tensile strength of drawn blends of PE/PET=70/30. 120
Figure 4-15: Microfibril diameters after extrusion and drawing using different sized dies. 121
Figure 4-16: For a PE/PET=70/30 blend the average microfibre diameter increases linearly with larger extrusion die diameter. Drawn microfibril diameters are smallest for 1-2 mm dies. 122
Figure 4-17: Tensile modulus of PE/PET=70/30 blend filament drawn at temperatures between 15°C and 90°C. 125
Figure 4-18: Tensile strength of PE/PET=70/30 blend filament drawn at temperatures between 15°C and 90°C. 125
Figure 4-19: Parameters used during calculation of the spherical and triangular velocity fields. 128
Figure 4-20: Model of spherical velocity field inside extrusion die - R_0 = 5 mm, R_f = 1 mm, α = 59° 129
Figure 4-21: Effect of changing die outlet size on spherical velocity field model - R_0 = 5 mm, α = 59°. 130
Figure 4-21 continued: Effect of changing die outlet size on spherical velocity field model - R_0 = 5 mm, α = 59°. 131
Figure 4-22: Model of triangular velocity field inside extrusion die - R_0 = 5 mm, R_f = 1 mm, $R\gamma$ = 2.5 mm, α = 59°. 132
Figure 4-23: Effect of changing die outlet size on triangular velocity field model - R_0 = 5 mm, $R\gamma$ = 3 mm, α = 59°. 133
Figure 4-24: Influence of the parameter $R\gamma$ in the triangular velocity field model - R_0 = 5 mm, R_f = 1 mm, α = 59°. 134
Figure 4-25: Effect of changing the convergence angle α for each velocity field model - R_0 = 5 mm, R_f = 1 mm, $R\gamma$ = 3 mm. 135
Figure 4-26: Shear rate of spherical velocity zone using Cartesian (left, middle) and Polar (right) co-ordinates. 136
Figure 4-27: Parameters used during calculation of the shear rate field. 137

Figure 4-28: Magnitude of stress acting on PET droplets in the converging die. Plot scaled to upper stability limit of 930 Pa. 138
Figure 5-1: Tensile stiffness of PE filaments with PET reinforcement loadings of 0, 10, 30 and 50%. 144
Figure 5-2: Tensile strength of PE filaments with PET reinforcement loadings of 0, 10, 30 and 50%. 145
Figure 5-3: MFC tensile specimens injection moulded from PP/PET. 148
Figure 5-4: Drawing speed versus draw ratio for a PP/PET=90/10 filament drawn at 140°C. 149
Figure 5-5: Changes in undrawn filament area with increasing PET for PP/PET blends. 150
Figure 5-6: Changes in undrawn filament area with increasing extruder temperatures for PP/PET blends. 150
Figure 5-7: Changes in the draw ratio with increasing levels of PET content for PP/PET blends. 151
Figure 5-8: Changes in the draw ratio with increasing drawing temperatures for PP/PET blends. 151
Figure 5-9: Fracture surface of injection moulded MFC specimen (left) and schematic explaining how this structure eventuates (right). 152
Figure 5-10: Tensile modulus results of MFCs from PP/PET. 153
Figure 5-11: Tensile strength results of MFCs from PP/PET. 153
Figure 5-12: Flexural modulus results of MFCs from PP/PET. 154
Figure 5-13: Flexural strength results of MFCs from PP/PET. 154
Figure 5-14: Impact strength results of MFCs from PP/PET. 155
Figure 5-15: Evidence of the changes occurring during injection moulding can be seen for the different blend ratios and moulding temperatures used. 157
Figure 5-16: Factor effects plots (left) and Q-Q plots (right) for the tensile modulus of MFCs from PP/PET 160
Figure 5-17: Factor effects plots (left) and Q-Q plots (right) for the tensile strength of MFCs from PP/PET 161
Figure 5-18: Factor effects plots (left) and Q-Q plots (right) for the flexural modulus of MFCs from PP/PET 162
Figure 5-19: Factor effects plots (left) and Q-Q plots (right) for the flexural strength of MFCs from PP/PET 163
Figure 5-20: Factor effects plots (left) and Q-Q plots (right) for the impact strength of MFCs from PP/PET 164
Figure 5-21: Tensile modulus (top) and tensile strength results (bottom) for neat PP, MFC from PP/PET=90/10 and MFC after compatibilisation with MAPP 169
Figure 5-22: Effect of reinforcing fraction on tensile modulus of MFCs from pelletised PE/PET 172
Figure 5-23: Effect of reinforcing fraction on tensile strength of MFCs from pelletised PE/PET. 173
Figure 5-24: Several different preparation techniques were used to create specimens to allow comparison of the effects of microfibril orientation in MFCs. 174
Figure 5-25: Effect of fibril orientation on tensile modulus of MFCs from PE/PET 175
Figure 5-26: Effect of fibril orientation on tensile strength of MFCs from PE/PET 175
Figure 6-1: Films compression moulded from PE/PET MFCs show the increasing difficulty in successfully forming a film as the levels of PET microfibrils in the blend increase from 0-60%. 185

Figure 6-2: Effect of PET content on permeability of MFC films from PE/PET. 185
Figure 6-3: Effect of draw ratio on permeability of MFC films from PE/PET. 187
Figure 6-4: Effect of draw ratio on permeability of MFC films from PP/PET. 187
Figure 6-5: Film thicknesses for each of the films created for permeability testing. 190
Figure 6-6: Oxygen permeability of films created using the manufacturing conditions of Table 6-5 (lower values are better barrier materials). 193
Figure 6-7: Factor effects plots for the oxygen permeability of MFC films from PE/PET. 195
Figure 6-8: Through-thickness microstructure of films containing 30% PET showing a variety of morphologies (a-d). Plain film (e) and microfibrils extracted from SO#8 (f) are also shown. 198
Figure 6-9: Tensile modulus of films made during experimental design investigation. 199
Figure 6-10: Tensile strength of films made during experimental design investigation. 200
Figure 6-11: Factor effects plots for the tensile modulus of films from PE/PET. 201
Figure 6-12: Factor effects plots for the tensile strength of films from PE/PET. 202
Figure 6-13: Oxygen permeability of neat PE and composite films before and after 12,000 hours ageing. 208
Figure 6-14: Relationship between oxygen permeability reduction and change in crystallinity. 210
Figure 6-15: Limiting cases for permeation using MFC parameters. Note that experimental reinforcement concentrations have been converted from wt. % to vol. %. 213
Figure 6-16: Nielsen models for two phase systems using MFC parameters. 214
Figure 6-17: Geometric model, Maxwell relation and Rayleigh relation applied to MFC parameters. 215
Figure 6-18: Applicable permeability models for filled and two phase polymer systems. 216
Figure 6-19: Normalised properties of composite films for each of the three test characteristics – oxygen permeability, tensile modulus and tensile strength. 219
Figure 7-1: The part model of the container as created in ProEngineer. 222
Figure 7-2: Assembled mould set. The injection point (arrow) and moulding cavity (circle) are indicated. 223
Figure 7-3: The completed mould is shown on the left. On the right are containers from it using LLDPE (clear) and MFCs with 10% (red), 15% (white) and 20% (blue) PET microfibrils. 224
Figure 7-4: Oxygen permeability testing rig for MFC containers. 225
Figure 7-5: Oxygen permeability of injection moulded containers. 225
Figure 7-6: pH of milk samples. 226
Figure 7-7: Visual quality of milk stored in plain LLDPE and MFC containers 6 days after expiry. The microfibril content of each container is shown on the lids. 227

NOMENCLATURE

Greek symbols

α	*Coefficient of thermal expansion*	*(mm/mm.°C)*
$\dot{\gamma}$	*Shear rate*	*(1/s)*
η	*Dynamic viscosity*	*(Pa.s)*
η_m	*Dynamic viscosity (matrix component)*	*(Pa.s)*
η_r	*Dynamic viscosity (reinforcing component)*	*(Pa.s)*
θ_{max}	*Reinforcement maximum packing fraction*	
κ	*Capillary number*	
κ_{cr}	*Critical capillary number*	
λ	*Viscosity ratio*	
ν	*Interfacial stress*	*(Pa)*
ν_{12}	*Interfacial tension coefficient*	*(Pa.m)*
σ	*Tensile stress*	*(MPa)*
σ_{crit}	*Critical stress*	*(MPa)*
σ_m	*Tensile stress (matrix component)*	*(MPa)*
σ_r	*Tensile stress (reinforcing component)*	*(MPa)*
σ_x	*Tensile stress at given test angle*	*(MPa)*
τ	*Shear stress*	*(Pa)*
Φ	*Diameter (of a fibre, fibril or droplet)*	*(μm) or (mm)*
Φ_{avg}	*Fibre, fibril or droplet diameter (average)*	*(μm) or (mm)*
Φ_{max}	*Fibre, fibril or droplet diameter (maximum stable)*	*(μm) or (mm)*
Φ_z	*Droplet diameter (maximum stable in vorticity direction)*	*(μm) or (mm)*

ψ	*Particle packing fraction factor*	

English symbols

A	*Cross-sectional area*	*(mm^2) or (m^2)*
B	*Die swell*	
C	*Concentration, or Crystallinity*	*(%)*
D	*Filament diameter, or Diffusion coefficient*	*(mm) (m^2/s)*
D_{avg}	*Filament diameter (average)*	*(mm)*
D_d	*Filament diameter (drawn)*	*(mm)*
D_u	*Filament diameter (undrawn)*	*(mm)*
d	*Die diameter*	*(mm)*
E	*Tensile modulus*	*(GPa)*
E_m	*Tensile modulus (matrix component)*	*(GPa)*
E_r	*Tensile modulus (reinforcing component)*	*(GPa)*
H_f	*Enthalpy of fusion*	*(J/g)*
H_f^*	*Enthalpy of fusion for 100% crystalline sample*	*(J/g)*
J	*Steady-state flux per unit area*	*(kg/m^2s)*
L	*Length (of a fibre, fibril or part)*	*(μm) or (mm)*
l	*Die land length, Film thickness*	*(mm), (μm)*
M_{gas}	*Molar amount of gas*	*(mol)*
m	*Mass fraction*	
P	*Permeability coefficient*	*(mol/m.s.Pa) or ($ml.mm/m^2.24hr.atm$)*
p	*Pressure*	*(kPa) or (atm)*
Q	*Peripheral roller speed during drawing*	*(m/s)*
R	*Reduction ratio*	
S	*Solubility constant*	
s	*Standard deviation*	
T	*Temperature*	*(°C)*

T_g	*Glass transition temperature*	*(°C)*
T_m	*Melting temperature*	*(°C)*
t	*Shearing time, or test duration*	*(s)*
$t`$	*Reduced time*	
t_{crit}	*Critical break-up time*	*(s)*
u	*Flow rate per unit area*	*(ml/m^2)*
V_f	*Volume fraction (fibres)*	
V_m	*Volume fraction (matrix component)*	
V_{perc}	*Percolation threshold*	
V_r	*Volume fraction (reinforcing component)*	
X	*Fibre tensile strength*	*(MPa)*
Y	*Transverse tensile strength*	*(MPa)*
y	*Response value*	

Glossary of Terms & Abbreviations

Polymer names

HDPE	*high density polyethylene*
LDPE	*low density polyethylene*
LLDPE	*linear low density polyethylene*
PE	*polyethylene*
PET	*poly(ethylene terephthalate)*
PP	*polypropylene*
ABS	*acrylonitrile-butadiene-styrene*
E-GMA	*ethylene-glycidyl methacrylate*
EVOH	*ethylene vinyl alcohol*
MAPP	*maleated polypropylene*
PA	*polyamide*
PBT	*poly(butylene terephthalate)*
PC	*polycarbonate*
PP-g-MA	*maleic anhydride-grafted polypropylene*
PS	*polystyrene*
PVC	*poly(vinyl chloride)*

Other abbreviations

ANOVA	*Analysis Of Variance*
ASTM	*American Society for Testing and Materials*
CDF	*Cumulative Density Function*
CLT	*Central Limit Theorem*
CM	*Compression Moulding*

DMTA	*Dynamic Mechanical Thermal Analysis*
DR	*Draw Ratio*
DSC	*Differential Scanning Calorimetry*
EDS	*Energy Dispersive X-ray Spectroscopy*
FTIR	*Fourier Transform Infra-red Spectroscopy*
IM	*Injection Moulding*
IUPAC	*International Union of Pure and Applied Chemistry*
MFC	*Microfibril Reinforced Composite*
MFR/MFI	*Melt Flow Rate / Melt Flow Index*
NFC	*Nanofibril Reinforced Composite*
NMR	*Nuclear Magnetic Resonance*
O_2GTR	*Oxygen Gas Transmission Rate*
PLM	*Polarizing Light Microscopy*
P'O_2	*Oxygen Permeance*
PO_2	*Oxygen Permeability Coefficient*
Q-Q plot	*Quantile-Quantile plot*
RO#	*Random Order Number*
RoM	*Rule of Mixtures*
SEM	*Scanning Electron Microscopy*
S/N ratio	*Signal-to-Noise Ratio*
SO#	*Standard Order Number*
STP	*Standard Temperature and Pressure*
TA	*Taguchi ANOVA*
TEM	*Transmission Electron Microscopy*
WAXS	*Wide Angle X-ray Spectroscopy*